Extending the dynamic slip boundary condition to variational multi-scale methods

By C. Carton de Wiart† AND S. M. Murman‡

This study focuses on extending the dynamic slip wall boundary condition to a high-order entropy-stable discontinuous Galerkin spectral-element solver. In this new wall-modeled approach, a wall Reynolds stress provided by a so-called slip/penetration velocity is added to the wall friction to compensate for the under-resolution at the wall. This slip/penetration velocity is derived from the properties of a differential filter and is applied through a Robin boundary condition. The extension of the method to compressible flows is presented, together with details of the Robin boundary condition in the framework of a discontinuous Galerkin method. The influence of the model free coefficient on the results is first analyzed. The method is assessed on a turbulent channel flow and compared to the no-slip approach as well as to an equilibrium wall model. A prototype dynamic procedure, to determine the free coefficient, is also presented. For optimized values of the coefficient, the slip/penetration wall model can reach similar accuracy to that of the equilibrium wall model on the channel flow. Nevertheless, it seems that the method is highly sensitive to the choice of the coefficient.

1. Introduction

As part of an effort within the NASA Aeronautics Transformational Tools and Technologies (TTT) project to improve the efficiency and accuracy of computational predictions of separated flows, a space-time Discontinuous Galerkin Spectral Element solver (DGSEM) has been developed over the past few years, as described by Diosady & Murman (2015). The solver uses a robust entropy-stable implementation, and a dynamic extension of the Variational Multiscale Method (VMM) developed by Hughes et al. (1998), in order to accurately predict the separated flow physics. The solver has been validated for Direct Numerical Simulation (DNS) and Large Eddy Simulation (LES) on canonical and industrial flows (see Garai et al. (2015); Diosady & Murman (2015)).

In this study, we propose extending the DGSEM/VMM approach to high Reynolds numbers using Wall Modeled LES (WMLES). Wall-modeling approaches are particularly interesting as they allow use a very coarse resolution in the boundary layer, even in the wall-normal direction, leading to a significant reduction in the number of mesh degrees of freedom. As shown in the recent review of Larsson et al. (2015), numerous wall models, mostly based on a wall-stress model, have been developed. The dynamic slip wall boundary condition, a recent approach developed by Bose & Moin (2014), captured our attention as it features very interesting properties. The method is consistent with the LES approach as it is based on a filtered state of the Navier-Stokes equations. This is not the case for typical wall-modeling approaches based on equilibrium and non-equilibrium boundary layer equations which can lead to undesired tuning of the LES parameters at

† NASA Postdoctoral Program, Universities Space Research Association
‡ NASA Ames Research Center

the near-wall. Also, the approach does not make any assumptions on the state of the boundary layer, which is one of the major problems of standard wall models, as stated by Park & Moin (2016). Finally, Bose & Moin (2014) showed that the method naturally recovers the unfiltered no-slip boundary condition when the mesh is sufficiently refined or when flow separation occurs.

This work aims to study further the properties of the dynamic slip boundary condition and evaluate its efficiency combined with the DGSEM/VMM approach for compressible flows. First, the slip/penetration wall boundary condition is presented, including its extension to compressible flows. The numerical methods are then briefly described, together with the treatment of the boundary conditions. The method is then evaluated on a turbulent channel flow at $Re_\tau = 544$. The influence of the free coefficient of the method is evaluated on two different mesh resolutions. The results are also compared to those of the DNS computed by Lee & Moser (2015) and to those obtained using an equilibrium wall model developed in the same DGSEM environment using the same mesh resolution. Finally, a prototype dynamic procedure for the free parameter of the method is tested.

2. The slip/penetration wall boundary condition

In this section the general idea of the slip/penetration wall is summarized first for incompressible flows. Next, the extension to compressible flows is presented and, lastly, the current implementation is described. For a more detailed analysis of the slip/penetration wall properties, the reader is referred to the original publication by Bose & Moin (2014).

2.1. *Background*

The slip/penetration wall, as first introduced by Bose & Moin (2014), is based on the assumption that the solution of the filtered Navier-Stokes equations would not necessarily provide a zero velocity at the wall, as is the case for wall-resolved LES or DNS. For instance, using the channel flow database at $Re_\tau = 2000$ of Lee & Moser (2015) and by filtering the velocity profile obtained using different filter lengths, one can see that the filtered velocity at the wall is not zero anymore and will increase together with the filter width, as seen in Figure (1).

Depending on the filtering approach, the solution of the filtered Navier-Stokes could therefore feature a non-zero velocity at the wall, also called the slip velocity. This slip velocity depends not only on the flow solution inside the domain but also on the grid size, which defines the filter size. Bose & Moin (2014) used the properties of a differential filter to derive a boundary condition that satisfies these properties. The differential filter, originally proposed by Germano (1986), is defined by the following equation

$$\bar{\phi} - \frac{\partial}{\partial x_i}\left(l_p \frac{\partial \bar{\phi}}{\partial x_i}\right) = \phi, \tag{2.1}$$

with $\bar{\phi}$ the filtered scalar ϕ and l_p a spatial variation of the filter width. Choosing $\phi = u_j$ (or $\phi = \rho u_j$ for compressible flows), the right-hand side of Eq. (2.1) vanishes to give a Robin boundary condition that can be used to define the slip velocity at the wall. This can be reinterpreted as follows: when running a computation using a deliberately coarse mesh, one seeks the solution of the filtered Navier-Stokes equations in which the coarse mesh acts as a differential filter, with the filter width defined as proportional to the mesh at the wall in the wall-normal direction.

As discussed in the next section, the method ensures a global non-penetration of the

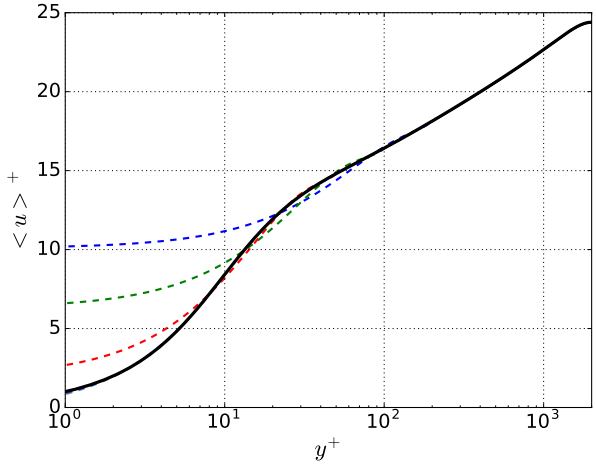

FIGURE 1. Filtered velocity profiles of the channel flow at $Re_\tau = 2000$ database of Lee & Moser (2015) using different filter sizes (dashed lines). Unfiltered profile is shown in thick line.

flow across the boundary. Nevertheless, the flow is allowed to penetrate the boundary locally and/or instantaneously, leading to the creation of Reynolds stress at the wall when the normal and the tangential velocities correlate. Hence, the term slip/penetration wall is preferred in this work to avoid any confusion with the standard slip wall boundary condition.

2.2. *Formulation for incompressible flows*

For incompressible flows, developing Eq. (2.1) at the wall where the velocity ($\phi = u_j$) is equal to zero, assuming l_p vanishes at the wall and using local coordinates aligned with boundary, the equation leads to

$$\bar{u_j}|_w - C\bar{\Delta}_n \left.\frac{\partial \bar{u}_j}{\partial n}\right|_w = 0, \tag{2.2}$$

with $C\bar{\Delta}_n = \left.\frac{\partial l_p}{\partial n}\right|_w$ the filter length scale at the wall. This value of $C\bar{\Delta}_n$ is a free parameter of the model but can be adjusted dynamically, as described by Bose & Moin (2014).

The continuity equation ensures that average normal velocity is zero at the wall. For instance, in the case of the plane turbulent channel flow, using $\langle\cdot\rangle$ as the average in the homogeneous directions (x and z) and y the wall normal direction, the continuity equation can be rewritten as

$$\left\langle \frac{\partial \bar{u}}{\partial x} \right\rangle\Big|_w + \left\langle \frac{\partial \bar{v}}{\partial y} \right\rangle\Big|_w + \left\langle \frac{\partial \bar{w}}{\partial z} \right\rangle\Big|_w = 0, \qquad \text{giving} \qquad \left\langle \frac{\partial \bar{v}}{\partial y} \right\rangle\Big|_w = 0, \tag{2.3}$$

as the two other derivatives will vanish for closed or periodic boundaries. This property is essential as it ensures no (average) penetration. Indeed, following our slip/penetration boundary condition, we have

$$\langle \bar{v} \rangle|_w - C\bar{\Delta}_n \left\langle \frac{\partial \bar{v}}{\partial y} \right\rangle\Big|_w = 0, \tag{2.4}$$

leading to $\langle \bar{v} \rangle|_w = 0$.

Also, when separation occurs, as $\partial \bar{u}_j/\partial n \to 0$, and when refining the mesh, as $C\Delta \to 0$, the method will recover a no-slip wall boundary condition, which is another interesting property of this method.

Using the Robin boundary condition defined in Eq. (2.2), Bose & Moin (2014) obtained very encouraging results for a turbulent channel flow at several Reynolds numbers and for an airfoil at low angle of attack at $Re = 1.6 \times 10^6$.

2.3. *Formulation for compressible flows*

As in incompressible flows, Eq. (2.1) can be rewritten as follows for compressible flows

$$\overline{\rho u}_j\big|_w - C\bar{\Delta}_n \frac{\partial \overline{\rho u}_j}{\partial n}\bigg|_w = 0. \tag{2.5}$$

After averaging the continuity equation in the wall-parallel directions, we obtain

$$\left\langle \frac{\partial \bar{\rho}}{\partial t} \right\rangle\bigg|_w + \left\langle \frac{\partial \overline{\rho v}}{\partial y} \right\rangle\bigg|_w = 0 \tag{2.6}$$

as the x- and z-direction terms disappear. Thus, for compressible flows, in contrast to incompressible flows, one cannot ensure $\langle \overline{\rho v} \rangle = 0$ by using Eq. (2.5) directly in the compressible equations. Similarly, one can show that for an adiabatic wall, Eq. (2.5) cannot ensure zero total energy flux and viscous work. This is confirmed as, when running tests using a naive implementation, the average density and total energy over the domain are increasing linearly in time.

To ensure a zero average mass flux at the wall, the average value of the normal derivative can be subtracted when computing the wall-normal momentum ρv from the slip/penetration wall, giving

$$\overline{\rho v}|_w = C\bar{\Delta}_n \left(\frac{\partial \overline{\rho v}}{\partial n} - \left\langle \frac{\partial \overline{\rho v}}{\partial n} \right\rangle \right), \tag{2.7}$$

leading to $\langle \overline{\rho v} \rangle|_w = 0$. This solution has the advantage of keeping the velocity fluctuations unchanged. Here, the average value inside each high-order element is chosen instead of computing the integral on the whole boundary, i.e., Eq. (2.7) is applied elementwise.

3. Entropy-stable Discontinuous Galerkin Spectral Element Method

The equations and their discretization are summarized in this section. For a more detailed analysis, the reader is referred to Diosady & Murman (2015).

The compressible Navier-Stokes equations are solved in a conservative form as

$$\boldsymbol{w}(\boldsymbol{v})_{,t} + \left(\boldsymbol{F}_i^I - \boldsymbol{F}_i^V \right)_{,x_i} = 0, \tag{3.1}$$

where $\boldsymbol{F}_i^I$ and $\boldsymbol{F}_i^V$ are the inviscid and viscous fluxes, respectively, and $\boldsymbol{w}(\boldsymbol{v})$ is the conservative state vector expressed as a function of the entropy variables $\boldsymbol{v}$. Equation (3.1) is discretized following a space-time discontinuous Galerkin method. The spatial domain is partitioned into non-overlapping elements κ, while the time is partitioned into time slabs $I^n = [t_n, t_{n+1}]$. Defining $\mathcal{V}_h = \left\{ \boldsymbol{\phi}, \boldsymbol{\phi}|_\kappa \in [\mathcal{P}(\kappa \times I)]^5 \right\}$, the space-time finite-element space consisting of piece-wise polynomial functions in both space and time on each ele-

ment, the weak form of Eq. (3.1) for a time slab $[n, n+1]$ is given by

$$\sum_{\kappa} \Bigg(\int_{I^n}\int_{\kappa} -\left(\boldsymbol{\phi}_{,t}\boldsymbol{w}(\boldsymbol{v}) + \boldsymbol{\phi}_{,x_i}\left(\boldsymbol{F}_i^I(\boldsymbol{v}) - \boldsymbol{F}_i^V(\boldsymbol{v}, \boldsymbol{v}_{,x_j})\right)\right) + \int_{I^n}\int_{\delta\kappa} [[\boldsymbol{\phi}]]\left(\mathcal{H}_i^I(\boldsymbol{v}^+, \boldsymbol{v}^-, n_i) - \left\{\boldsymbol{F}_i^V(\boldsymbol{v}, \widetilde{\boldsymbol{v}_{,x_j}})\right\} n_i\right) - \left\{\boldsymbol{\phi}_{,x_i}\boldsymbol{F}_i^V(\boldsymbol{v}, [[\boldsymbol{v}]])\right\} + \int_{\kappa} \boldsymbol{\phi}(t_{n+1}^-)\ \boldsymbol{w}(\boldsymbol{v}(t_{n+1}^-))\Bigg) = \sum_{\kappa}\int_{\kappa} \boldsymbol{\phi}(t_n^+)\ \boldsymbol{w}(\boldsymbol{v}(t_n^-)), \qquad \forall \boldsymbol{\phi}_i \in \mathcal{V}_h, \tag{3.2}$$

where $[[a]] = a^+ n_i^+ + a^- n_i^-$ and $\{a\} = (a^+ + a^-)/2$ are the jump and the average operators, respectively. $\widetilde{a_{x_j}} = a_{,x_j} - \eta_e[[a]]$ is the lifted gradient, with η_e the lifted parameter. When discretizing using the entropy variables, we seek a solution $\boldsymbol{w}(\boldsymbol{v})$, $\boldsymbol{v} \in \mathcal{V}_h$, allowing entropy-stability for the numerical scheme using the right choice of numerical flux function (see Diosady & Murman (2015)). In this work, the inviscid flux $\mathcal{H}_i^I$ is computed using the method of Ismail & Roe (2009) and the viscous contribution using the BR2 method by Bassi & Rebay (2000).

For the boundary conditions, a fictitious boundary state $\boldsymbol{v}_b$ must be provided in order to impose the inviscid flux, leading to

$$\boldsymbol{f}^I(\boldsymbol{v}_b, \boldsymbol{v}, \boldsymbol{\phi}) = \int_{I^n}\int_{\delta\kappa} \boldsymbol{\phi}\mathcal{F}_i^I(\boldsymbol{v}, \boldsymbol{v}_b, n_i). \tag{3.3}$$

The inviscid flux can be computed either through a Riemann solver ($\mathcal{F}_i^I(\boldsymbol{v}, \boldsymbol{v}_b, n_i) = \mathcal{H}_i^I(\boldsymbol{v}, \boldsymbol{v}_b, n_i)$), as for the interface flux, or by directly imposing the flux from the boundary state ($\mathcal{F}_i^I(\boldsymbol{v}, \boldsymbol{v}_b, n_i) = \boldsymbol{F}_i^I(\boldsymbol{v}_b)n_i$). Similarly, the viscous boundary flux can be computed by assuming that the gradients of the boundary state are equal to the gradient of the interior state $\boldsymbol{v}_{b,x_j} = \boldsymbol{v}_{,x_j}$, allowing the same formulation to be retrieved as the interface flux

$$\boldsymbol{f}^V(\boldsymbol{v}_b, \boldsymbol{v}, \boldsymbol{\phi}) = \int_{I^n}\int_{\delta\kappa} \boldsymbol{\phi}\left(-\left\{\boldsymbol{F}_i^V(\boldsymbol{v}_b, \widetilde{\boldsymbol{v}_{b,x_j}})\right\} n_i\right) - \left\{\boldsymbol{\phi}_{,x_i}\boldsymbol{F}_i^V(\boldsymbol{v}_b, [[\boldsymbol{v}]])\right\}. \tag{3.4}$$

Another option is to directly use the interior value

$$\boldsymbol{f}^V(\boldsymbol{v}_b, \boldsymbol{v}, \boldsymbol{\phi}) = \int_{I^n}\int_{\delta\kappa} \boldsymbol{\phi}\left(-\boldsymbol{F}_i^V(\boldsymbol{v}, \widetilde{\boldsymbol{v}_{,x_j}})n_i\right) - \boldsymbol{\phi}_{,x_i}\boldsymbol{F}_i^V(\boldsymbol{v}, [[\boldsymbol{v}]]). \tag{3.5}$$

Finally, the viscous flux can also be imposed directly using

$$\boldsymbol{f}^V(\boldsymbol{v}_b, \boldsymbol{v}, \boldsymbol{\phi}) = \int_{I^n}\int_{\delta\kappa} \boldsymbol{\phi}\left(-\mathcal{F}_i^V(\boldsymbol{v}_b)n_i\right). \tag{3.6}$$

Eq. (3.3) can be combined with Eqs. (3.4), (3.5) or (3.6) to apply Dirichlet, Neumann or Robin boundary conditions. For instance, the no-slip Dirichlet boundary condition can be recovered by constructing $\boldsymbol{v}_b$ using $\rho u_j = 0$ and by taking ρ and ρE from the interior. The inviscid flux can then be directly imposed, as $\mathcal{F}_i^I(\boldsymbol{v}, \boldsymbol{v}_b, n_i) = \boldsymbol{F}_i^I(\boldsymbol{v}_b)n_i$, while the viscous flux can be computed using Eq. (3.5). For an equilibrium wall model, the friction computed by the wall model can be directly imposed through a Neumann boundary condition using Eq. (3.6), while Eq. (3.3) satisfies a slip wall.

The Robin boundary condition for the slip/penetration wall is set by constructing the boundary state $\boldsymbol{v}_b$ from Eq. (2.5) and using ρ and ρE from the interior state to close the system, in a way similar to that in the no-slip boundary condition. The inviscid flux is then computed using a modified Riemann solver, $\mathcal{F}_i^I(\boldsymbol{v}, \boldsymbol{v}_b, n_i) = \mathcal{H}_i^I(\boldsymbol{v}, \boldsymbol{v}_b, n_i)$,

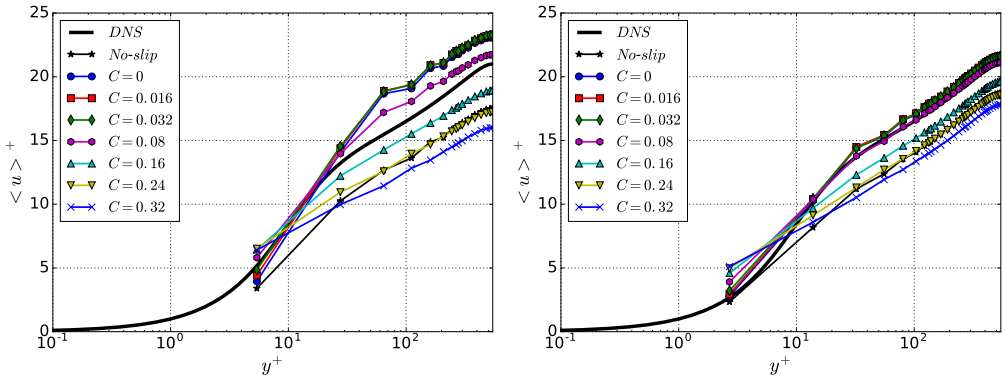

FIGURE 2. Channel flow at $Re_\tau = 544$. 32^3 (left) and 64^3 (right) dof.

that removes the inviscid flux from the mass and energy equations, and the viscous flux is computed using Eq. (3.5). The Robin boundary condition is then imposed as a Dirichlet-type boundary condition. One could also implement the Robin boundary as a Neumann boundary condition by directly prescribing the viscous flux as a function of the interior state, following Eq. (2.5). Nevertheless, the Dirichlet type is preferred here as the method will converge to a no-slip boundary condition ($\rho u_j \to 0$) when $C\Delta \to 0$, whereas the Neumann type would be undefined, with $\frac{\partial \rho u_j}{\partial y} \to \infty$ for $C\Delta \to 0$.

4. Validation on a turbulent channel flow

The fully developed turbulent flow between two parallel walls separated by a distance 2δ in the y-direction is considered. The flow is assumed periodic in the wall-normal directions (x and z). The Reynolds number is chosen as $Re_\tau = u_\tau \delta/\nu = 544$, with $u_\tau = \sqrt{\tau_w/\rho}$ the friction velocity based on the wall shear stress τ_w. The friction Reynolds number is imposed through a constant forcing in the x-momentum equation using the pressure gradient $\frac{dp}{dx} = -\frac{\tau_w}{\delta}$. A Mach number of $M = 0.1$ is also chosen to match the incompressible conditions of the reference DNS of Lee & Moser (2015). Two coarse meshes are considered, containing 32^3 and 64^3 degrees of freedom (dof), respectively, using a constant distribution in the three directions (wall-normal mesh not stretched), giving a mesh size at the wall of $\Delta y^+ = 68$ and $\Delta y^+ = 34$, respectively. All computations are performed using eighth order polynomials.

4.1. *Calibration of* $C\Delta$

The sensitivity of the method to its free parameter, $C\Delta$, is first analyzed. To this end, values of C are taken ranging from $C = 0$ (no-slip) to $C = 1.6$, using Δ as the mesh size in the wall-normal direction ($\Delta = h_0/N$, with h_0 the first high-order cell height and N the order of the polynomial). For this configuration, computations were shown to be unstable for values of $C > 0.32$. Figure (2) shows the resulting velocity profiles using $C \leq 0.32$ for the two mesh resolutions. For both mesh resolutions, the best results are obtained using values of the coefficient around $C \approx 0.08 - 0.1$. When modifying the coefficient, the velocity profile is shifted up and down, while roughly keeping the same slope in the logarithmic region. The position of the logarithmic region on the ordinate can therefore be used to measure the accuracy of the results. This measurement can be done by extrapolating the slope of the profile in the logarithmic region on the $y^+ = 1$ location

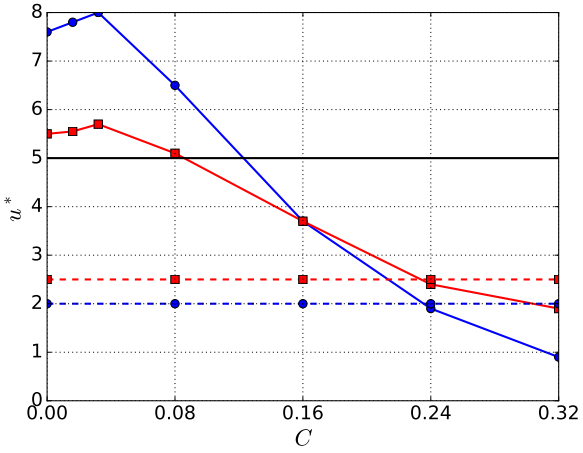

FIGURE 3. Channel flow at $Re_\tau = 544$. Position of the logarithmic region of the velocity profile. DNS target at $u^* = 5$. 32^3 dof mesh (circles) and 64^3 dof mesh (squares). Slip/penetration (solid lines) and no-slip (dash lines).

(defined here as u^*). For the DNS of Lee & Moser (2015), the logarithmic law that intersects the $y^+ = 1$ location at $u^* = 5$, as represented by the dashed line in Figure (2). As shown on Figure (3), the result obtained using $C = 0$ does not correspond to those of the no-slip wall, as it would normally be expected. Indeed, the slip/penetration wall is imposed through a Riemann solver while the no-slip wall imposes directly the flux at the wall from the boundary values. When first increasing the value of C, the position of the curve moves slightly upward. When the value of C is high enough to generate significant Reynolds stress at the wall ($< -u'v' >$), the curve then moves downward. The results show that the method seems more sensitive to the choice of the C parameter when the mesh is coarse (Δ is large), which could cause robustness problems for severely under-resolved computations.

4.2. *Comparison with equilibrium wall-model*

The method is now compared to an equilibrium wall model on the 64^3 dof mesh. As described in Carton de Wiart *et al.* (2014), the equilibrium model is based on an analytical law of the wall, such as the Reichardt profile, and computes a wall friction from the values of the fluid at the top of the first cell, in this case $y+ = 136$. The slip/penetration wall computation is performed using the optimum value of the slip/penetration length, i.e. $C = 0.08$. Figure (4) shows the resulting velocity profile together with the three diagonal components of the Reynolds stress. Both the slip/penetration wall and the equilibrium wall model greatly improve the results compared with those of the no-slip wall. The velocity profile is well captured and the fluctuations are in good agreements with those of the DNS. The major differences between the boundary conditions occur in the first cell. Whereas the equilibrium wall model tends to keep increasing the fluctuations when moving closer to the wall, the slip/penetration wall will tend to a value below the fluctuation peak, in between the no-slip and the equilibrium wall model curves. Outside the first element (for $y^+ > 136$), the results are almost indistinguishable.

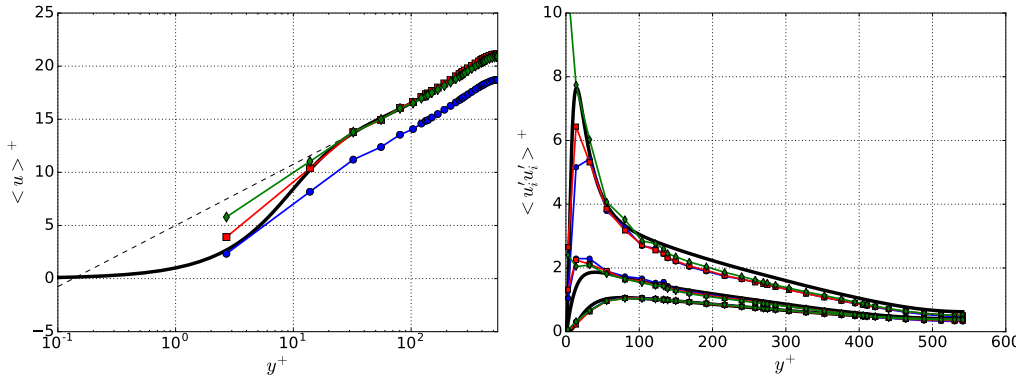

FIGURE 4. Channel flow at $Re_\tau = 544$. Left: mean velocity profile. Right: mean velocity fluctuations. DNS of Lee & Moser (2015)(thick line), no-slip wall (circle), slip/penetration wall (square) and equilibrium wall model (diamond).

5. Towards a dynamic slip/penetration wall

As the method is very sensitive to the choice of the coefficient $C\Delta$, a dynamic procedure is required to apply the method to arbitrary flows. To this end, Bose & Moin (2014) derived a method to dynamically compute the slip length. Unfortunately, this method is not directly applicable to our discretization of the compressible Navier-Stokes equations. A prototype dynamic procedure compatible with our approach is described here.

The slip/penetration wall boundary condition uses the Reynolds stress generated by the slip/penetration velocity together with the approaching friction at the wall, computed from the filtered Navier-Stokes equations. The filtered field now features an inviscid flux $\boldsymbol{f}^I$, and a viscous flux $\boldsymbol{f}^V$, computed using Eq. (3.3) and Eqs. (3.5), respectively. Assuming that the optimal C is not dependent on the choice of Δ, it is possible to derive a dynamic procedure based on the assumption that the integral of the boundary fluxes will remain the same regardless of the mesh resolution. Denoting with h the current resolution and by applying a second projection operator to a coarser test space, H, the following equality should be recovered for an optimum value of C

$$\boldsymbol{f}^I(\bar{\boldsymbol{v}_b}^h, \bar{\boldsymbol{v}}^h, \bar{\boldsymbol{\phi}}^h) + \boldsymbol{f}^V(\bar{\boldsymbol{v}_b}^h, \bar{\boldsymbol{v}}^h, \bar{\boldsymbol{\phi}}^h) = \boldsymbol{f}^I(\bar{\boldsymbol{v}_b}^H, \bar{\boldsymbol{v}}^H, \bar{\boldsymbol{\phi}}^H) + \boldsymbol{f}^V(\bar{\boldsymbol{v}_b}^H, \bar{\boldsymbol{v}}^H, \bar{\boldsymbol{\phi}}^H), \quad (5.1)$$

assuming that this optimal C is equal at both the nominal and the test levels. Eq. (5.1) depends directly on the value of C as the boundary state, $\boldsymbol{v}_b = \boldsymbol{v}_b(C\Delta, \boldsymbol{v}_{,x_i})$, is constructed from the slip/dynamic wall equations. As the filter is constructed by projecting the solution of the nominal space of order h to the coarse space of order H, Δ^H can be related to Δ^h by $\Delta^H = \Delta^h \frac{H}{h}$. Instead of computing the integral of the fluxes on the whole boundary, we assume that a local boundary face carries enough information to satisfy Eq. (5.1). An optimal value of C, constant on each boundary face, can therefore be computed by applying a least-squares approach to Eq. (5.1). A useful property of the dynamic procedure is that it will reverse to no-slip $C = 0$ when the flow is resolved.

This method has been applied *a priori* on the channel flow, running using the optimum value of the coefficient $C = 0.08$. At each time-slab and for each boundary face, the coefficient is computed from the dynamic procedure but is not applied. Figure (5) shows the temporal evolution of the mean value of the coefficient C. The temporal average of the coefficient is equal to $C = 0.1$, which is close to the value that gives the best results with respect to the DNS. Nevertheless, the fluctuations of the coefficient are extremely

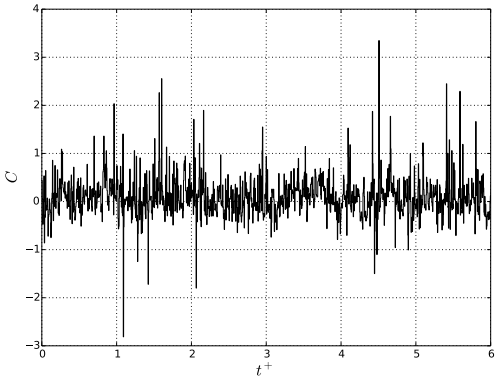

FIGURE 5. Channel flow at $Re_{\tau=544}$. Temporal evolution of the mean coefficient C extracted *a priori* from the results of the computation using the optimum value of the coefficient $C = 0.08$.

large and can even go to negative value, which makes the procedure inapplicable to a real dynamic computation. Also, the maxima of the coefficient are above $C = 3$, whereas the method has been shown unstable for $C > 0.32$.

6. Conclusions

In this study, the slip/penetration wall boundary condition has been successfully applied to a compressible DGSEM solver. A new Robin boundary condition has been derived and the method has been applied to a turbulent channel flow at $Re_\tau = 544$. The method is very sensitive to the choice of the slip length, and a larger value of the slip length make the method unstable, as the Reynolds stress generated at the wall keeps growing while the resolved wall friction tends to zero. Nevertheless, optimum values of the coefficient can be found. For these values, the method shows an accuracy similar to that of equilibrium wall models for the channel flow benchmark. Close to the wall, the fluctuations are even closer to the DNS as the method constrains the velocity at the wall. Finally, a new version of the dynamic procedure, better adapted to the current discretization, has been derived. The *a priori* test on the channel flow shows that the average coefficient obtained using the dynamic procedure is close to the optimum value. Nevertheless, the large fluctuations of the coefficient make it difficult to apply to more realistic cases. In order to improve the dynamic procedure, several options are considered. Tests on the behavior of the filter have shown that the filtered velocity at the wall could be negative, leading to negative values of the slip/penetration coefficient. The projection operator could therefore be improved by putting more weight on the values away from the wall. The coefficient could also be averaged in time to get a more stabilized value. A version that compares the fluxes at the same filter level could also be derived. These ideas remain to be evaluated in future work.

The method should also be further analyzed on higher Reynolds numbers, using more realistic WMLES grid specifications with coarser mesh sizes. The first tests have already showed robustness issues as the method seems more sensitive to the choice of C when Δ is large.

Using a robust dynamic procedure, the slip wall could solve most of the challenges of wall modeling, as the method can recover the no-slip wall boundary condition for separation or when the mesh is sufficiently fine to resolve the flow structures. Also, it

does not depend on the position of the input of the wall model, as is typically the case for equilibrium or non-equilibrium wall models. Indeed, the method depends only on the solution at the wall as the model is applied through a Robin boundary condition.

Acknowledgments

The authors would like to thank Sanjeeb Bose and Jane (Hyunji) Bae for their help in understanding the dynamic slip wall approach. Research was supported by an appointment to the NASA Postdoctoral Program at the NASA Ames Research Center, administered by Universities Space Research Association under contract with NASA.

REFERENCES

Bassi, F. & Rebay, S. 2000 GMRES Discontinuous Galerkin solution of the compressible Navier-Stokes equations. In *Discontinuous Galerkin Methods: Theory, Computation and Applications.* Springer **26**, 197–208.

Bose, S. T. & Moin, P. 2014 A dynamic slip boundary condition for wall-modeled large-eddy simulation. *Phys. Fluids.* **26**, 015104.

Carton de Wiart, C., Frère, A. & Hillewaert, K. 2014 Towards wall-modeled implicit LES with a Discontinuous Galerkin Method. *10th International ERCOFTAC Symposium on Engineering Turbulence Modelling and Measurements.*

Diosady, L. & Murman, S. 2015 Higher-order methods for compressible turbulent flows using entropy variables. *53rd AIAA Aerospace Sciences Meeting.*

Garai, A., Diosady, L. T., Murman, S. M., & Madavan, N. 2015 DNS of flow in a low-pressure turbine cascade using a Discontinuous-Galerkin spectral-element method. *In Proceedings of ASME Turbo Expo 2015.*, GT2015-42773.

Germano, M. 1986 Differential filters for the large eddy simulation of turbulent flows. *Phys. Fluids.* **29**, 1755–1766.

Hughes, T. J. R., Feijoo, G. R., Mazzei, L., & Quincy, J.-B. 2015 The variational multi-scale method - a paradigm for computational mechanics. *Comput. Methods Appl. Math.* **166**, 3–24.

Ismail, F. & Roe, P. L. 2009 Entropy-consistent Euler flux functions II: entropy production at shocks. *J. Comput. Phys.* **228**, 5410–5436.

Larsson, J., Kawai, S., Bodart, J. & Bermejo-Moreno, I. 2016 Large eddy simulation with wall-modeled wall-stress: recent progress and future directions. *Mech. Eng. Reviews.* **3**, 15-00418.

Lee, M. & Moser, R. D. 2015 Direct numerical simulation of turbulent channel flow up to $Re_\tau = 5200$. *J. Fluid Mech.* **774**, 395–415.

Park, G. I. & Moin, P. 2016 Numerical aspects and implementation of a two-layer zonal wall model for LES of compressible turbulent flows on unstructured meshes. *J. Comput. Phys.* **305**, 589–603.